Numerical Study of the Unified Kadomtsev-Petviashvili Equation

by

Yongze Chen

and

Philip L. F. Liu

RESEARCH REPORT NO. CACR-95-04

April, 1995

Center for Applied Coastal Research
Ocean Engineering Laboratory
University of Delaware
Newark, DE 19716

Numerical Study of the Unified Kadomtsev-Petviashvili Equation

by

Yongze Chen[1]

and

Philip L.-F. Liu[2]

[1]Center for Coastal Studies, Scripps Institution of Oceanography, La Jolla, CA 92093, USA
[2]School of Civil Engineering, Cornell University, Ithaca, NY 14853, USA

Abstract

In this paper, we numerically investigate the unified Kadomtsev–Petviashvili (uKP) equation derived by Chen & Liu (1995), which describes weakly nonlinear and dispersive surface and interfacial waves propagating primarily in the longitudinal direction of a slowly rotating channel with varying topography and sidewalls. This paper focuses on the effect of topography on the propagation of a solitary wave in a stationary channel and a Kelvin solitary wave in a rotating channel. We find that in the absence of rotation, an oblique incident solitary wave propagating over a three-dimensional shelf in a straight wide channel will eventually develop into a series of uniform straight-crested solitary waves, together with a train of small oscillatory waves propagating upstream; with proper phase shifts, the shapes of these final two-dimensional solitary waves coincide with the shapes of those final solitary waves emerged from a corresponding normal incident solitary wave propagating over the corresponding two-dimensional shelf. In a two-layered rotating channel, the variation of topography does not have much effect on the propagation of a Kelvin solitary wave of depression, whereas it can have a significant influence on the propagation of a Kelvin solitary wave of elevation. Explanations for these numerical findings are given.

1 Introduction

Ever since Kadomtsev & Petviashvili (1970) first wrote down their equation as an evolution equation for weakly nonlinear and dispersive water waves propagating over a constant depth in a predominant direction, this equation has been a topic of research for a quarter of century. The Kadomtsev–Petviashvili (KP) equation possesses a number of remarkable properties and becomes the prototype equation representing completely integrable evolution equations in two spatial dimensions (Ablowitz

& Clarkson 1991). To extend the applicability of the original KP equation, various generalizations have appeared (see Akylas' (1994) review paper on recent advances in understanding certain three-dimensional, nonlinear free surface long-wave phenomena which can be described by the KP-type equations). Most recently, Chen & Liu (1995) (hereafter referred to as CL) gave the derivation of the unified KP (uKP) equation for weakly nonlinear and dispersive surface and interfacial waves propagating predominantly in the longitudinal direction of a slowly rotating channel with varying topography and sidewalls, and a weak steady background current field. Their result was a generalization of all previous work within the context of surface and interfacial waves. They also found the complete integrability conditions for the uKP equation and obtained integral invariants corresponding to conservation of mass and of energy for waves propagating in a varying channel.

For completely integrable evolution equations, there are several powerful techniques to obtain many classes of analytical solutions (soliton, multisoliton, periodic solutions, etc.), such as inverse scattering transform, Bäcklund transformations, Hirota's method and symmetry reductions. Unfortunately, the complete integrability conditions for the uKP equation are very restrictive. They require that no rotation exist, the variation of topography be weak and behave like a linear function in the transversal direction (so does the background current field if it is present). Moreover, the sidewall boundary conditions usually will interfere with the integrability. Therefore, to apply the uKP equation to more complex situations, in which it is not completely integrable, we need to solve the equation numerically.

Although several numerical schemes have been proposed for the KdV equation (for finite-difference methods and spectral methods see Taha & Ablowitz 1984; for finite-element methods see Mitchell & Schoombie 1984), numerical methods for KP-type equations do not seem to have been so successful. Pierini (1986) presented an

implicit, three-time level, finite-difference scheme to solve the regularized KP equation (which is not completely integrable) for weakly three-dimensional wave propagation in a rectangle channel. Katsis & Akylas (1987*a*) proposed an explicit, conditionally stable finite-difference scheme for the KP equation and extended this scheme to the rotation-modified KP (rmKP) equation (1987*b*). Grimshaw & Tang (1990) developed a different numerical scheme for the rmKP equation by using the Petrov–Galerkin finite-element method. All these numerical schemes made use of the assumption that solutions are locally confined in an infinite domain. Recently, Wineberg *et al.* (1991) presented an implicit spectral method for the KP equation. Because the Fourier transform was used, their method can only be applied to spatial periodic wave propagation problems.

All the numerical schemes mentioned above were developed based on the constant-coefficient KP or rmKP equations. Therefore, the effects of topography on three-dimensional solitary wave propagation in a wide straight channel (the channel width is much larger than the water depth) have not been studied before.[1] In this paper we study this problem by solving the uKP equation numerically. The Petrov–Galerkin finite-element method is used to develop an accurate numerical scheme for the uKP equation. The numerical scheme is first tested through simple examples, in which either analytical solutions or numerical solutions given by other researchers are available. Then, it is used to study solitary wave propagation in a stationary channel and Kelvin solitary wave propagation in a rotating channel. In the numerical study, we focus on the effect of topographic variation on the wave propagation. We find that in the absence of rotation, an oblique incident solitary wave (with an angle of incidence smaller than the critical angle for the Mach reflection to occur according to Miles'

[1] Mathew & Akylas (1990) derived the KP equation and the sloping sidewall boundary conditions to study the propagation of long, weakly nonlinear water waves along a uniform cross-section channel bounded by sloping sidewalls.

theory (1977a, b)) propagating over a three-dimensional shelf in a straight channel will eventually develop into a series of uniform straight-crested solitary waves, together with a train of small oscillatory waves propagating upstream. Moreover, with proper phase shifts, the shapes of these final two-dimensional solitary waves coincide with the shapes of those final solitary waves evolved from a corresponding normal incident solitary wave propagating over the corresponding two-dimensional shelf. The two-dimensionalization is due to the alternating development of a stem wave along the left- and right-hand sidewall, which gradually reduces the amplitude and speed differences between the waves near the left-hand sidewall and waves near the right-hand sidewall and eventually leads to the formation of uniform straight-crested solitary waves spanning the entire channel width. We also find that in a two-layered rotating channel, the topographic variation has little effect on the propagation of a Kelvin solitary wave of depression: the wave patterns look similar with or without the presence of a shelf, whereas it can have a significant influence on the propagation of a Kelvin solitary wave of elevation. The reason is that in the absence of rotation, the corresponding KdV solitary wave of depression cannot experience fission under the weak nonlinearity and dispersion assumption, whereas the corresponding KdV solitary wave of elevation can easily undergo fission without violating this assumption.

2 Numerical scheme

In the absence of the background current field, the uKP equation reads (see CL)

$$\sqrt{C}\frac{\partial}{\partial X}\left(\sqrt{C}\frac{\partial \eta}{\partial \xi}\right)+\frac{3C^2}{4}D_{-2}\frac{\partial^2\eta^2}{\partial\xi^2}+\frac{\alpha D_1}{6}\frac{\partial^4\eta}{\partial\xi^4}+\frac{C^2}{2}\frac{\partial^2\eta}{\partial Y^2}-\frac{\beta^2}{2}\eta + \frac{\rho^- BC^2}{2(h^-)^2}\frac{\partial^2\eta}{\partial\xi^2}=0, \tag{2.1a}$$

with

$$C(X) = \left(\rho^-/h^- + \rho^+/h^+\right)^{-1/2}, \tag{2.1b}$$

$$D_n(X) = \rho^-(h^-)^n + (-1)^{(n-1)}\rho^+(h^+)^n, \quad (n = 1, -2). \tag{2.1c}$$

In (2.1), η is the departure of the interface from its undisturbed equilibrium level. The independent variables X and Y are the slow horizontal coordinates in the longitudinal and transversal directions of a two-layered rotating channel, respectively, whereas ξ is the characteristic coordinate moving at the leading-order local linear-long-wave speed C. The depth of the upper layer is $H^+ = h^+$, whereas the depth of the lower layer is given by $H^- = h^-(X) + \epsilon B(X, Y)$, where ϵ is a small parameter measuring the weak nonlinearity. The densities of the upper and lower layers are ρ^+ and ρ^-, respectively. Parameters α and β measure the relative importance of the dispersion and rotation effects to the nonlinear effect. The boundary conditions along the vertical sidewalls $Y = Y_R(X)$ and $Y = Y_L(X)$ are:

$$\frac{\partial \eta}{\partial Y} + \frac{\beta}{C}\eta = \frac{1}{C}\frac{\mathrm{d}Y}{\mathrm{d}X}\frac{\partial \eta}{\partial \xi} \quad \text{on} \quad Y = Y_R(X),\ Y_L(X). \tag{2.2}$$

We remark that in (2.1) and (2.2), X can be viewed as a time-like coordinate, whereas ξ can be viewed as a space-like coordinate.

For initial-boundary-value problems, unless Y_R and Y_L are both constant, the domain of a solution to the uKP equation in the (ξ, Y)-plane changes at different X (see (2.2)). To carry out numerical computations in a fixed domain, we introduce the following transformation:

$$\zeta = \sqrt{C}\eta, \quad \bar{Y} = (Y - Y_R)/W, \tag{2.3a}$$

where

$$W(X) = Y_L(X) - Y_R(X) \tag{2.3b}$$

is the width of the channel. Under this transformation, the uKP equation (2.1) and the boundary conditions along the sidewalls (2.2) become

$$\frac{\partial^2\zeta}{\partial X\partial\xi} + \frac{3\sqrt{C}}{4}D_{-2}\frac{\partial^2\zeta^2}{\partial\xi^2} + \frac{\alpha D_1}{6C}\frac{\partial^4\zeta}{\partial\xi^4} + \frac{C}{2W^2}\frac{\partial^2\zeta}{\partial\bar{Y}^2} - \frac{\beta^2}{2C}\zeta + \frac{\rho^- BC}{2(h^-)^2}\frac{\partial^2\zeta}{\partial\xi^2} - \frac{1}{W}(Y_R' + \bar{Y}W')\frac{\partial^2\zeta}{\partial\xi\partial\bar{Y}} = 0, \tag{2.4a}$$

$$\frac{\partial\zeta}{\partial\bar{Y}} + \frac{\beta W}{C}\zeta = \frac{W}{C}Y_R'\frac{\partial\zeta}{\partial\xi} \quad \text{on} \quad \bar{Y} = 0, \tag{2.4b}$$

$$\frac{\partial\zeta}{\partial\bar{Y}} + \frac{\beta W}{C}\zeta = \frac{W}{C}Y_L'\frac{\partial\zeta}{\partial\xi} \quad \text{on} \quad \bar{Y} = 1, \tag{2.4c}$$

where $' = \mathrm{d}/\mathrm{d}X$. Note that the domain of a solution to problem (2.4) in the $(\xi, \bar{Y})$-plane is fixed and no term involving $(h^-)'$ appears in (2.4), which may be significant in computations if $(h^-)'$ is large in some region.

To solve (2.4) numerically as an initial-boundary-value problem, we have to replace the infinite domain $-\infty < \xi < +\infty$ with a finite computational domain $\xi_{-\infty} \le \xi \le \xi_{+\infty}$ and impose appropriate boundary conditions at $\xi = \xi_{\pm\infty}$. According to the linear dispersion relation of the uKP equation, the group velocity is always negative. Thus, for a sufficient large $\xi_{+\infty}$, it is permissible to set ζ and its derivatives equal to zero at $\xi = \xi_{+\infty}$. However, at $\xi = \xi_{-\infty}$, a radiation boundary condition is needed to avoid artificial reflection. Since the uKP equation is a nonlinear evolution equation with variable coefficients for three-dimensional wave propagation, finding a suitable radiation boundary condition at $\xi = \xi_{-\infty}$ is difficult. Here we adopt an *ad hoc* assumption that ζ and its derivatives equal to zero at $\xi = \xi_{-\infty}$, i.e. solutions are locally confined. For any local confined solution, it must satisfy the following restriction (see

CL):

$$\int_{-\infty}^{+\infty} \eta \mathrm{d}\xi = F(X) \exp\left(-\beta Y/C\right), \qquad X \geq 0, \tag{2.5}$$

where F is an arbitrary function of X. Thus, the assumption requires that all initial conditions should satisfy (2.5) at $X = 0$. If this constraint is violated, disturbances may propagate to $-\infty$ in finite time according to the group velocity expression (Katsis & Akylas 1987*b*; Grimshaw & Melville 1989; Akylas 1994), and thus the *ad hoc* assumption is no longer valid. Numerical tests confirm that if the initial condition satisfies (2.5), we can choose the finite interval $\xi_{-\infty} \leq \xi \leq \xi_{+\infty}$ sufficiently large to keep ζ very small near $\xi = \xi_{\pm\infty}$ within the 'time' interval $X \in [0, X_0]$ of interest.

Following Pierini (1986), Katsis & Akylas (1987*b*) and Grimshaw & Tang (1990), we first convert equation (2.4a) into an integral-differential equation

$$\begin{aligned} &\frac{\partial \zeta}{\partial X} + \frac{3\sqrt{C}}{4} D_{-2} \frac{\partial \zeta^2}{\partial \xi} + \frac{\alpha D_1}{6C} \frac{\partial^3 \zeta}{\partial \xi^3} + \frac{\rho^- BC}{2(h^-)^2} \frac{\partial \zeta}{\partial \xi} \\ &\qquad = \int_{\xi}^{+\infty} \left(\frac{C}{2W^2} \frac{\partial^2 \zeta}{\partial \bar{Y}^2} - \frac{\beta^2}{2C} \zeta \right) \mathrm{d}\xi + \frac{Y_R' + \bar{Y} W'}{W} \frac{\partial \zeta}{\partial \bar{Y}}, \end{aligned} \tag{2.6}$$

where $\zeta \to 0$ as $\xi \to +\infty$ has been used. Equation (2.6) has the form of a forced KdV equation and methods developed for the KdV equation can be modified to deal with (2.6) in principle. The main difficulty is how to discretize the terms on the right-hand side of (2.6). For the KdV equation, from the point of view of accuracy and efficiency, the Petrov–Galerkin finite-element method performs better than finite difference methods and spectral methods (Sanz-Serna & Christie 1981; Mitchell & Schoombie 1984). Thus, we use the Petrov–Galerkin finite-element method to develop a numerical scheme for (2.6). The Petrov–Galerkin finite-element method was also used by Grimshaw & Tang (1990) for the rmKP equation. The main difference between their scheme and ours is the treatment for the terms on the right-hand side of (2.6). We use the extended trapezoidal rule to calculate the integral on the right-

hand side of (2.6) and use second-order central finite differences to approximate the $\bar{Y}$-derivatives (see Chen (1995) for details about the numerical scheme).

The accuracy of the numerical scheme is verified by two tests. The first one is a normal incident solitary wave propagating over a two-dimensional shelf and the second one is a solitary wave propagating over a three-dimensional weak and gentle topography in a curved channel. The former was numerically studied by Johnson (1972), whereas the latter has analytical solutions (see CL). In both tests, our numerical results agree excellently with the known solutions (see Chen 1995). Thus, we are confident that our numerical scheme can give accurate results as long as disturbances remain localized. We then use the numerical scheme to study the propagation of a solitary wave in a stationary channel and a Kelvin solitary wave (a KdV solitary wave multiplied by an exponential function in the transversal direction so that the constraint (2.5) is met) in a rotating channel. In numerical computations, domain $[\xi_{-\infty}, \xi_{+\infty}]$ is always chosen large enough to ensure that the disturbances near $\xi = \xi_{\pm\infty}$ are very small, at least within the computational 'time' interval of interest $X \in [0, X_0]$. Thus, the *ad hoc* assumption that ζ and its derivatives equal to zero at $\xi = \xi_{-\infty}$ is held. For each case, the relative errors between the numerical evaluated (by trapezoidal rule) first-order (when the rotation is absent) and second-order integral invariants (see (4.5) and (4.6) in CL) and the exact values at different X are never in exceed of 0.5%. The constraint (2.5) is also monitored across the channel.

3 Solitary wave propagation in a stationary channel

In the absent of rotation, numerical results are presented for surface solitary waves propagating in a straight channel. For convenience, we set $\alpha = 6$ in the uKP equation.

The initial condition, which satisfies the constraint (2.5) at $X = 0$, is given by

$$\eta(\xi, 0, Y) = 8\mathrm{sech}^2\left(\xi + \sqrt{6}\, lY/2\right), \tag{3.1}$$

where l is a constant, determining the direction of the incident solitary wave. Computational parameters: $\Delta\xi = 0.1$, $\Delta\bar{Y} = 0.05$ and $\Delta X = 0.25 \times 10^{-3}$ are used for each numerical example presented in this section. We first study the transformation of an oblique incident solitary wave in a uniform channel and then investigate the effect of topographic variation on the solitary wave propagation.

3.1 Oblique incident solitary wave propagation in a uniform channel

Figure 1 shows the transformation of an oblique incident solitary wave given by (3.1) with $l = 1.0$ propagating in a channel with constant depth and width ($h = W = 1$) at different X. In the moving frame, at first, a Mach stem wave normal to the left sidewall develops. The crest along the left sidewall gradually increases, while the crest along the right sidewall decreases (cf. figure 1 *a* with 1 *b*). Due to the nonlinear effect, the speed of the crest along the left sidewall is greater than that along the right sidewall. Thus, the wave crest near the left sidewall speeds up, catches up with and surpasses the rest of the wave crest (see figures 1 *c* and 1 *d*). This leads to a smaller opposite (compared with the original oblique incidence) inclination. Another weaker Mach reflection along the right sidewall begins to develop. As a result, the speed of the wave near the right sidewall begins to increase, while the speed of the wave near the left sidewall decreases. Soon, the maximum wave amplitude switches from the left to the right sidewall (see figure 1 *e*). The speed of the wave near the right sidewall continues to increase until it catches up with the wave near the left sidewall

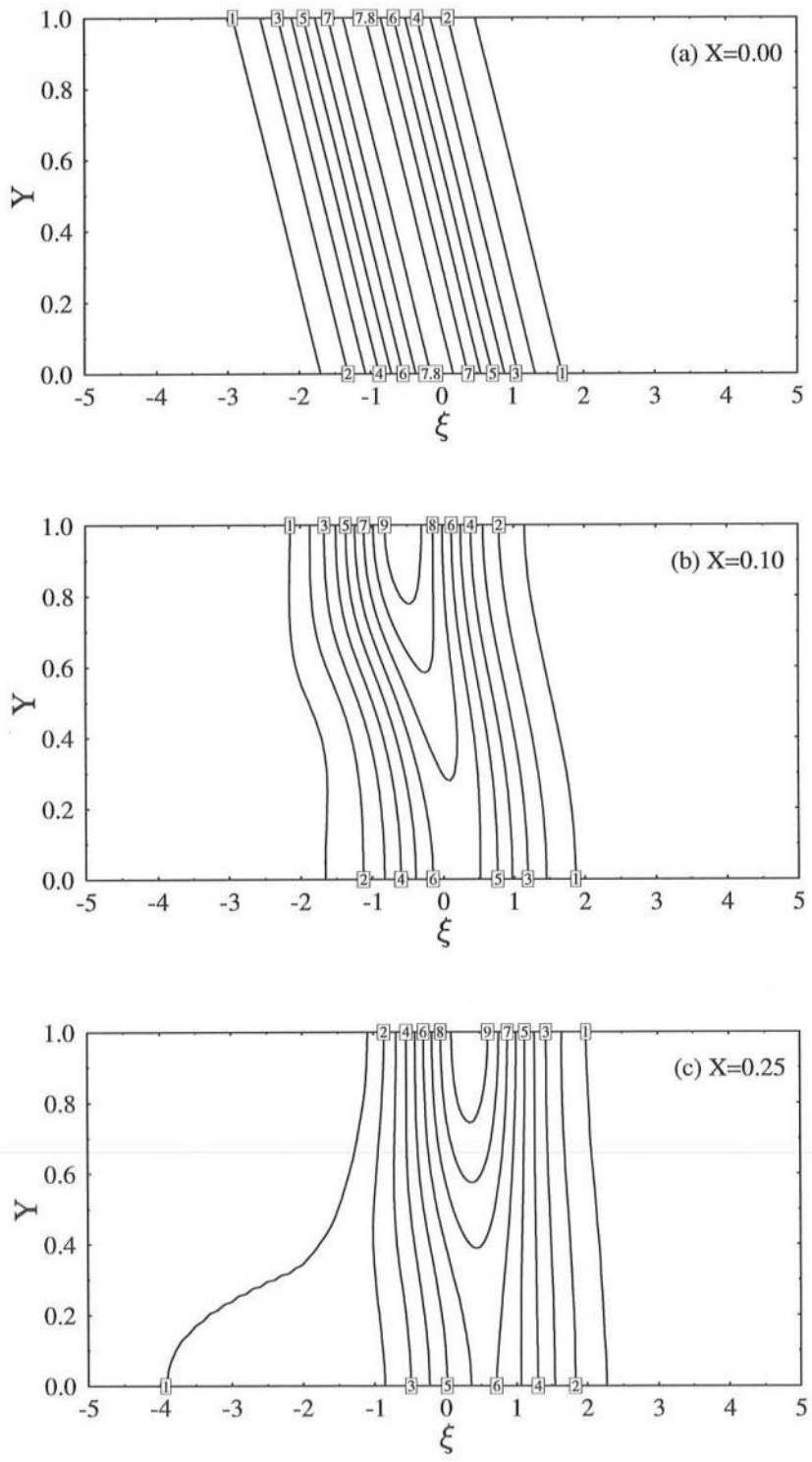

Figure 1: Contour plots of an oblique incident solitary wave propagating in a uniform channel at different X.

Figure 1 (Continued)

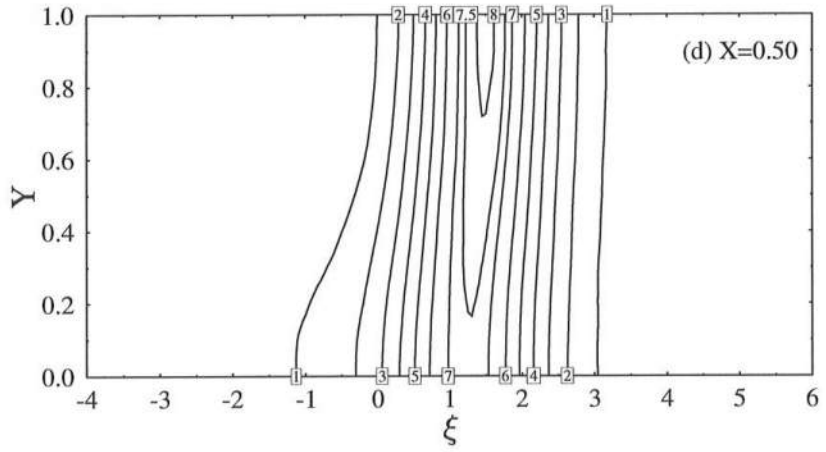

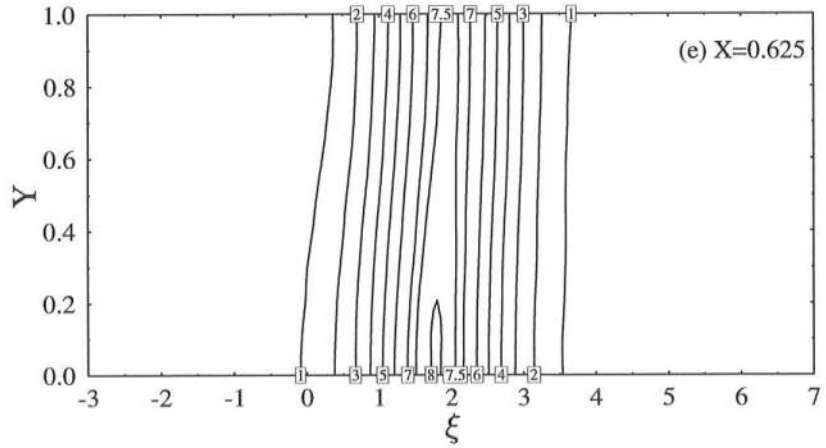

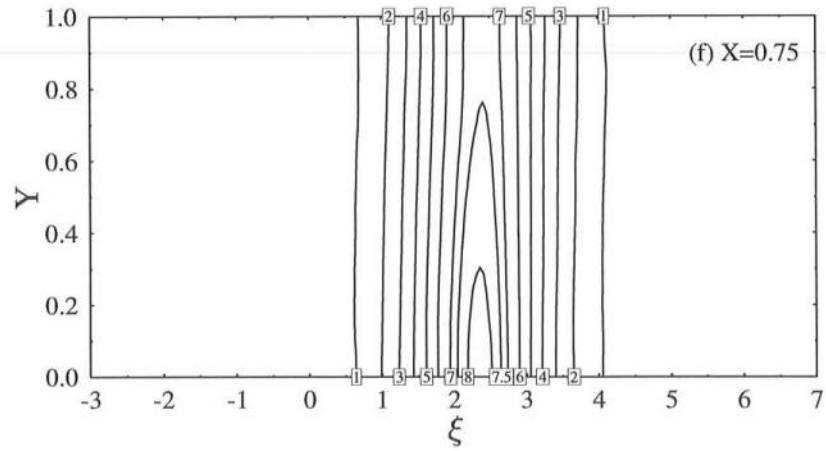

Figure 1 (Continued)

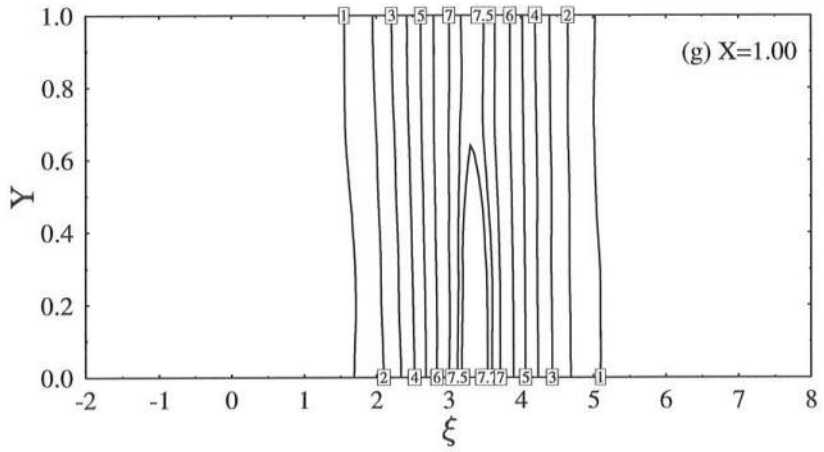

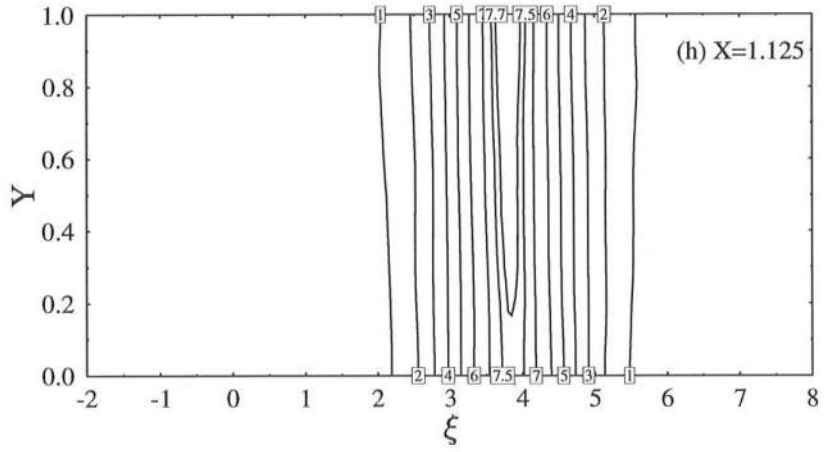

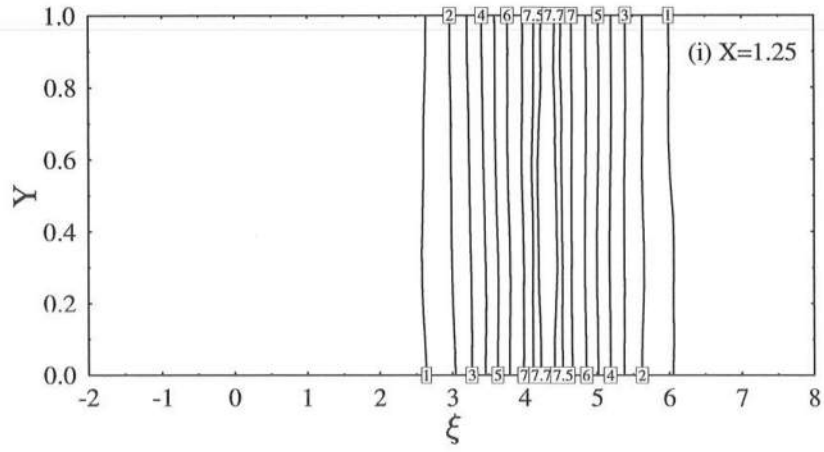

(see figure 1 f). Then, another even smaller inclination (after each catch-up, the amplitude difference between the crests along the left and right sidewalls is further reduced) forms and the speed of the crest along the left sidewall begins to increase due to the Mach reflection, while the speed along the right sidewall decreases (cf. figure 1 f with 1 g). This process is repeated until a uniform straight-crested solitary wave forms (see figure 1 i). During this so called 2-D adjustment process, a train of 3-D small-amplitude waves is generated and propagates upstream (see figure 2). In the oscillatory tail, the region near the centerline is rather calm compared to the regions close to each sidewall. Figure 3 shows the elevation along the centerline of the channel at $X = 1.25$ and the exact solitary-wave solution given by (3.1) ($l = 0$) with the same peak location. From figures 2 and 3, one can conclude that after the oscillatory wave disperses towards the upstream, the final state of the oblique incident solitary wave is a 2-D solitary wave with the same amplitude as that of the incident wave.

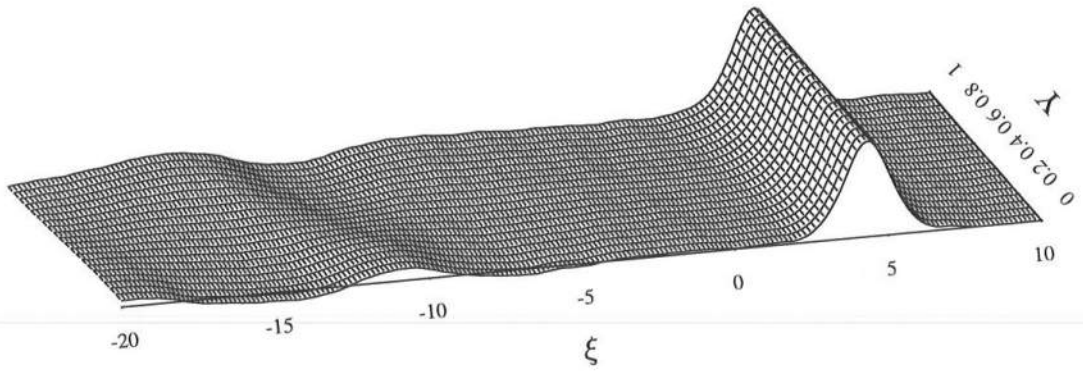

Figure 2: Surface displacement of an oblique incident solitary wave propagating in a uniform channel at $X = 1.25$.

For the same oblique incident solitary wave propagating in a wider uniform channel ($W = 1.6$), similar phenomenon is observed. However, in a wider channel, since the distance between the crests along the right and left sidewall is larger initially, it takes

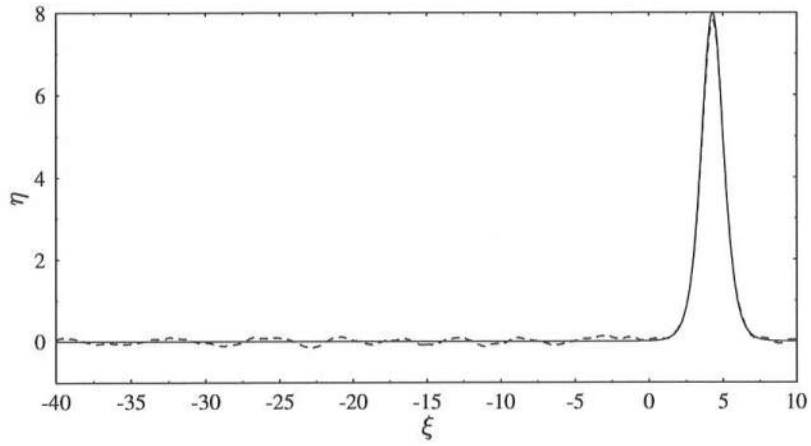

Figure 3: Comparison between the elevation of an oblique incident solitary wave at $X = 1.25$ (- - -) and the exact solitary-wave solution (——) with the same peak location along the centerline of the channel.

a longer time for the wave near the left-hand sidewall to catch up with the wave near the right-hand sidewall. More importantly, when it happens, the amplitude difference between the crests along the left-hand and right-hand walls is also larger in a wider channel, because there is more time for the stem wave to develop before the interference of the right-hand sidewall. Consequently, it needs more time to form the final 2-D solitary wave.

For an oblique incident solitary wave given by (3.1), according to Miles' theory (1977a, b), the Mach reflection along a vertical wall will occur when the angle of incidence in the (ξ, Y)-plane is smaller than the critical angle $\arctan(2\sqrt{6}) = 78.46°$. In the previous case ($l = 1.0$ in (3.1)), the angle of incidence is $\arctan(\sqrt{6}/2) = 50.77°$. For the same incident solitary wave with a larger angle of incidence propagating in the same channel, similar phenomenon is observed: a uniform straight-crested solitary wave emerges as the result of the 2-D adjustment process described before, followed by a train of small oscillatory waves propagating upstream. But, as the angle of incidence gets closer to the critical angle, it takes more time for the final 2-D solitary wave to

emerge and the maximum amplitude (achieved at the sidewalls) in the oscillatory tail increases. The critical angle for the Mach reflection to occur (i.e. for the resonance of the incident and reflected solitary waves to occur) is proportional to the square root of the incident wave amplitude (Miles 1977a, b). Thus, if the angle of incident remains the same, the angle of incidence of a smaller incident solitary wave is relatively closer to the corresponding critical angle. Therefore, for different size of solitary waves propagating in the same channel with the same angle of incidence, the emergence of the final 2-D solitary wave takes a longer time for a smaller incident wave. This agrees with our numerical results.

In conclusion, for an oblique incident solitary wave propagating in a uniform channel, as long as the angle of incidence is smaller than the critical angle for the Mach reflection to occur according to Miles' theory (1977a, b), the alternating development of a stem wave along the left-hand and right-hand sidewall will lead to the emergence of a 2-D solitary wave, together with an oscillatory tail propagating upstream. The 2-D adjustment process takes a longer time for an angle of incidence closer to the corresponding critical angle and in a wider channel. In other words, if the initial state is further away from the final 2-D state (but has a limit), it needs more time to reach the final state. We remark that for an oblique incident Gaussian-shaped wave, similar 2-D adjustment process was reported by Pierini (1986), who numerically solved the regularized KP equation to describe the wave propagation in a rectangle channel.

We now further investigate what happens to an oblique solitary wave if it propagates along a channel with 2-D topography.

3.2 Oblique incident solitary wave propagation in a channel with 2-D topography

The 2-D adjustment mechanism occurs not only in channels with constant depth, but also in channels with 2-D varying topography. For an oblique incident solitary wave given by (3.1) with $l = 1.0$ propagating over a varying topography given by

$$h(X) = 1 - 0.2\tanh(X/2) \tag{3.2}$$

in a straight channel, we observe that the same 2-D adjustment mechanism leads to the formation of a uniform straight-crested solitary wave (which has a higher amplitude than the incident wave dose due to the decrease of the water depth and the conservation of energy), together with a train of oscillatory waves (see figure 4). Note that the depth given by (3.2) deviates significantly from the greatest eigen-depth value, $3^{-4/9} = 0.614$, predicted by the soliton fission law found by Tappert & Zabusky (1971), Johnson (1973) and Ono (1972). For a corresponding normal incident solitary wave propagating over this topography, no fission occurs (the solitary wave deforms into a taller one, followed by an oscillatory tail).

Now we study the same oblique incident wave propagating over a 2-D shelf which allows fission to occur. The shelf is given by

$$h(X) = \begin{cases} 1, & X \leq 0, \\ 0.5\left[1 + D + (1 - D)\cos(2\pi X)\right], & 0 < X \leq 0.5, \\ D, & X > 0.5, \end{cases} \tag{3.3}$$

where $D = 3^{-4/9} = 0.614$ (the greatest eigen-depth value) is chosen so that for a normal incident solitary wave given by (3.1) with $l = 0$ propagating over this shelf, two solitary waves will eventually emerge in the constant depth region of the shelf

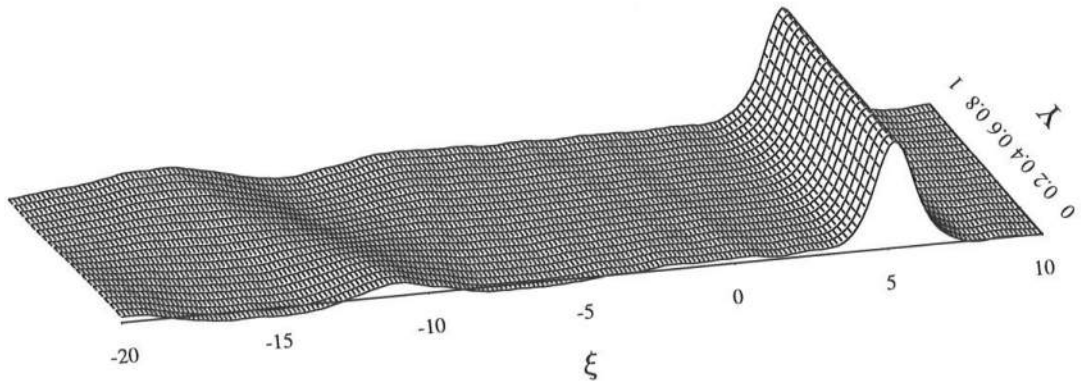

Figure 4: Surface displacement of an oblique incident solitary wave propagating in a channel with 2-D topography given by (3.2) at $X = 1.25$.

according to the fission law.

Figure 5 shows the transformation of the oblique incident solitary wave propagating over the 2-D shelf at different X. One can see that as the wave propagates into the decreasing depth region ($0 \leq X \leq 0.5$), first a stem wave develops along the left sidewall and then the wave near the left-hand sidewall catches up with and surpasses the wave near the right-hand sidewall (see figure 5 *a–c*). Next, a stem wave along the right-hand sidewall begins to develop, which results in the increase of the wave amplitude along the right-hand sidewall. In the meantime, fission begins to occur on each vertical plane parallel to the sidewalls. When the waves arrive at the constant depth region ($X = 0.5$), the first wave looks almost two-dimensional, while the second one is definitely three-dimensional (see figure 5 *d*). After entering to the constant depth region ($X > 0.5$), these two waves eventually develop into two uniform straight-crested solitary waves through the 2-D adjustment process (see figures 5 *e–f* and 6), trailed by a train of 3-D small oscillatory waves (the maximum wave amplitude is at the sidewalls) propagating upstream. Figure 7 shows the centerline elevation of the oblique and the corresponding normal incident solitary wave propagating over the

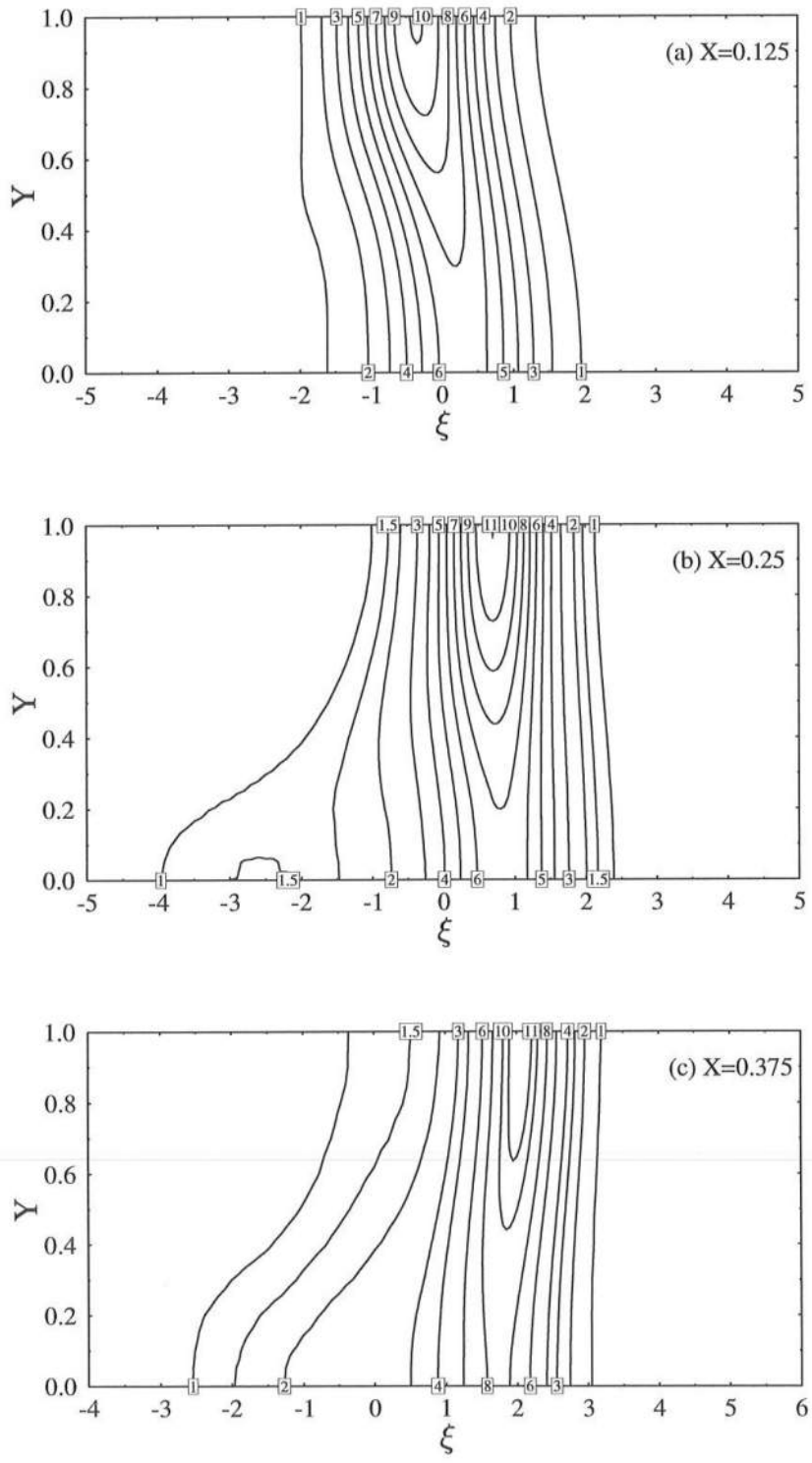

Figure 5: Contour plots of an oblique incident solitary wave propagating over a 2-D shelf in a straight channel at different X.

Figure 5 (Continued)

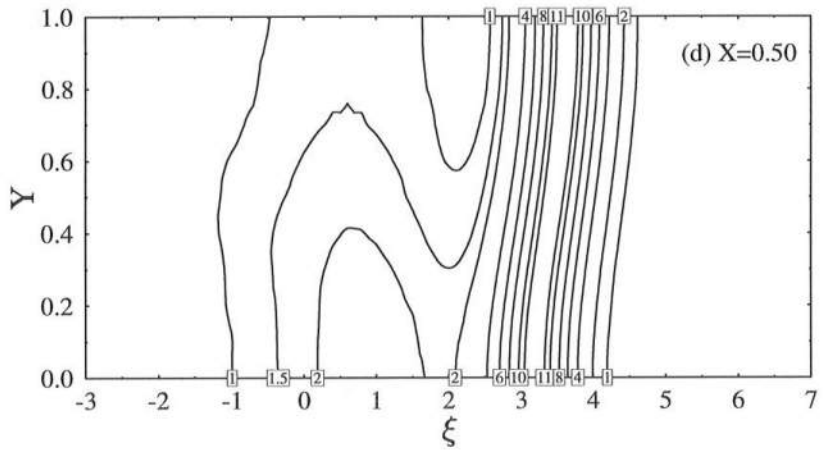

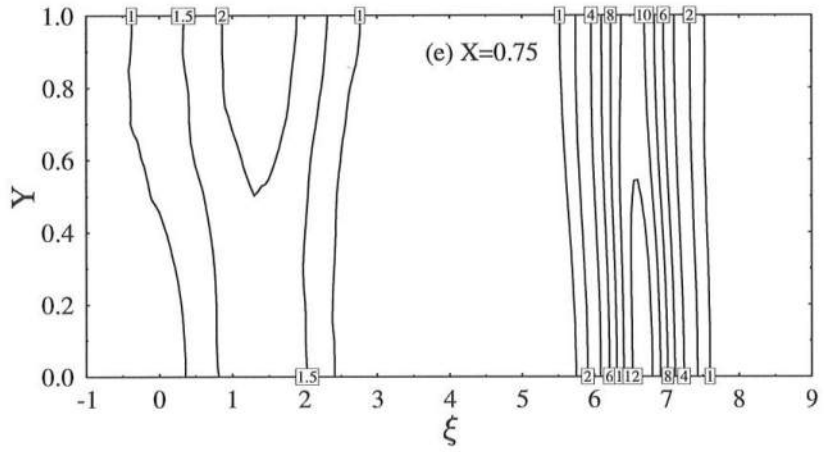

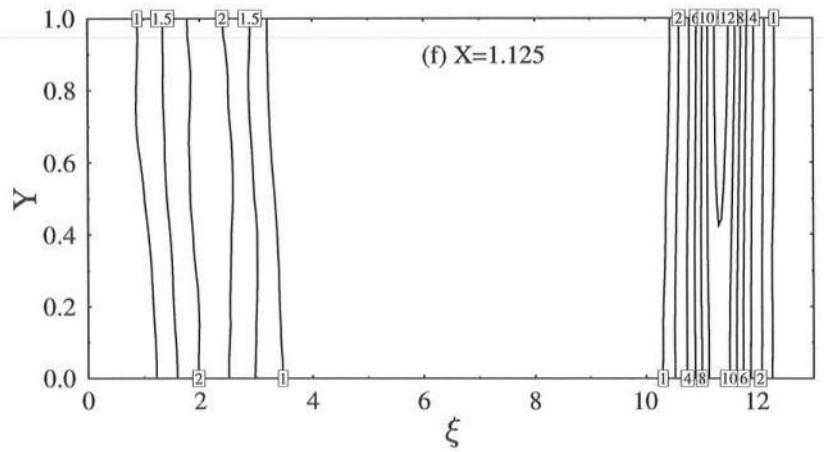

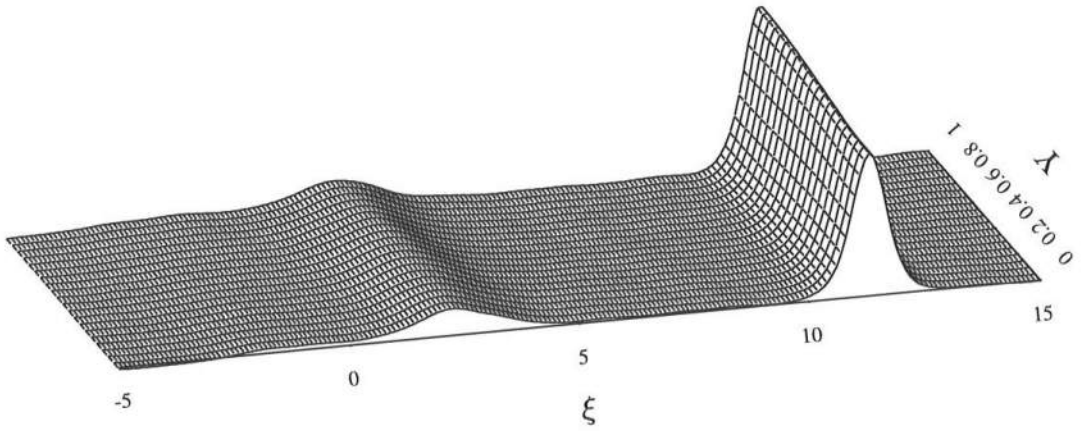

Figure 6: Surface displacement of an oblique incident solitary wave propagating over a 2-D shelf given by (3.3) at $X = 1.125$.

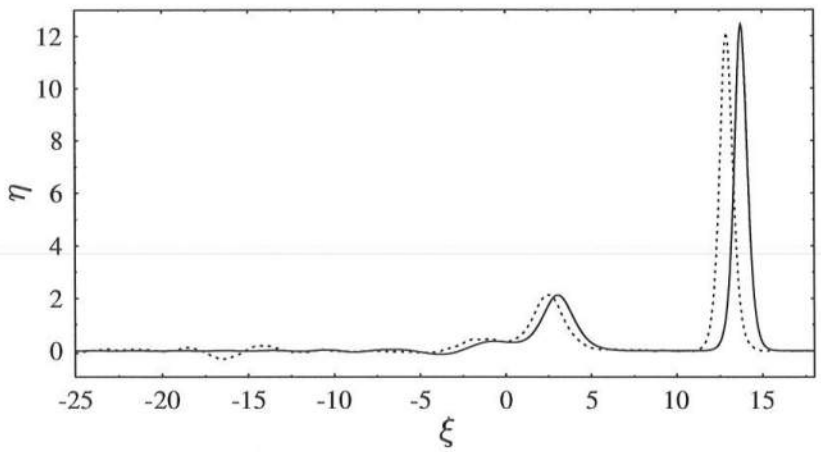

Figure 7: Centerline elevation of a normal and an oblique incident solitary wave propagating over a 2-D shelf given by (3.3) at $X = 1.25$. ——, normal incident; $\cdots$, oblique incident.

same shelf at $X = 1.25$. From this figure, one can see that with proper phase shifts, the shapes of the two solitary waves evolved from the oblique incident solitary wave propagating over the 2-D shelf coincide with the shapes of those two solitary waves emerged from the corresponding normal incident solitary wave propagating over the same shelf (strictly speaking, the second solitary wave is not a perfect solitary wave due to the finite length (in terms of X) of the shelf, which generates an oscillatory tail immediately followed the second solitary wave).

Because of the significant increase in computational work, we do not carry out further investigation on an oblique incident solitary wave propagating over a shallower 2-D shelf which allows stronger fission to occur. Nevertheless, based on the numerical results presented in this subsection, it is very logical to expect that in general, an oblique incident solitary wave (with an angle of incidence smaller than the critical angle for the Mach reflection to occur according to Miles' theory (1977a, b)) propagating over a 2-D shelf in a straight channel will eventually develop into a series of uniform straight-crested solitary waves, together with a train of oscillatory wave propagating upstream. With proper phase shifts, the shapes of these final 2-D solitary waves coincide with the shapes of those final solitary waves evolved from a corresponding normal incident solitary wave propagating in the same channel.

In the following subsection, we further investigate the effect of the transversal variation of a 3-D shelf on the propagation of a solitary wave in a straight channel.

3.3 Solitary wave propagation in a channel with a 3-D shelf

We first study a normal incident solitary wave given by (3.1) with $l = 0$ propagating over a 3-D shelf described by

$$H = h(X) + \epsilon B(X, Y), \tag{3.4a}$$

where $h(X)$ is given by (3.3) and B is given by

$$B(X,Y) = \begin{cases} 0, & X \leq 0, \\ 16\left[\cos(4\pi X) - 1\right](Y - Y^2), & 0 < X \leq 0.5, \\ 0, & X > 0.5. \end{cases} \tag{3.4b}$$

Note that the shelf has continuous first derivative everywhere (see figure 8).

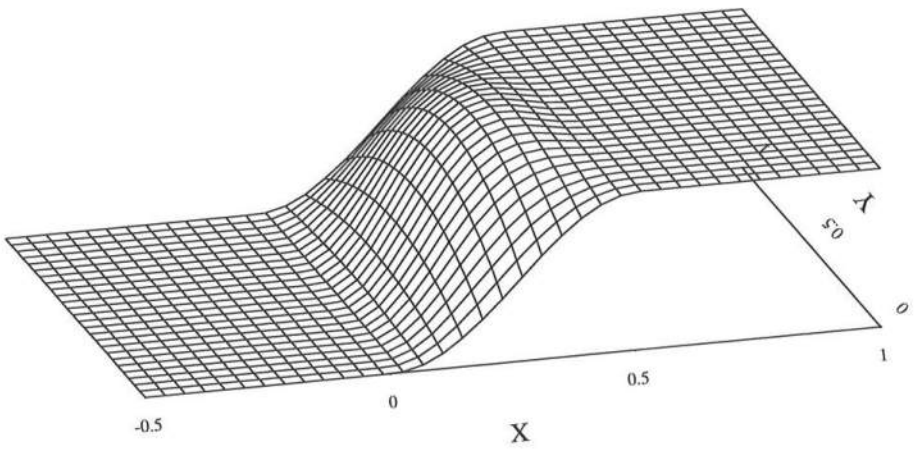

Figure 8: The shape of the 3-D shelf given by (3.4) ($\epsilon = 0.02$).

Figure 9 shows the transformation of the solitary wave propagating over the 3-D shelf at different X. The variation of the shelf in the Y-direction in the region $0 \leq X \leq 0.5$ destroys the original 2-D structure of the solitary wave. But once the wave passes over this changing depth region and enters to the constant depth region ($X > 0.5$), two uniform straight-crested solitary waves emerge as a result of fission and the 2-D adjustment process. It is worth mentioning that the second solitary wave is evolved from the wave with strong 3-D structure (see figure 9 *b*).

Figure 10 shows the centerline elevation of the same normal incident solitary wave propagating over the 2-D shelf ($B = 0$ in (3.4a)) and over the 3-D shelf at $X = 1.0$ (the maximum amplitude of the oscillatory tail is along the centerline for

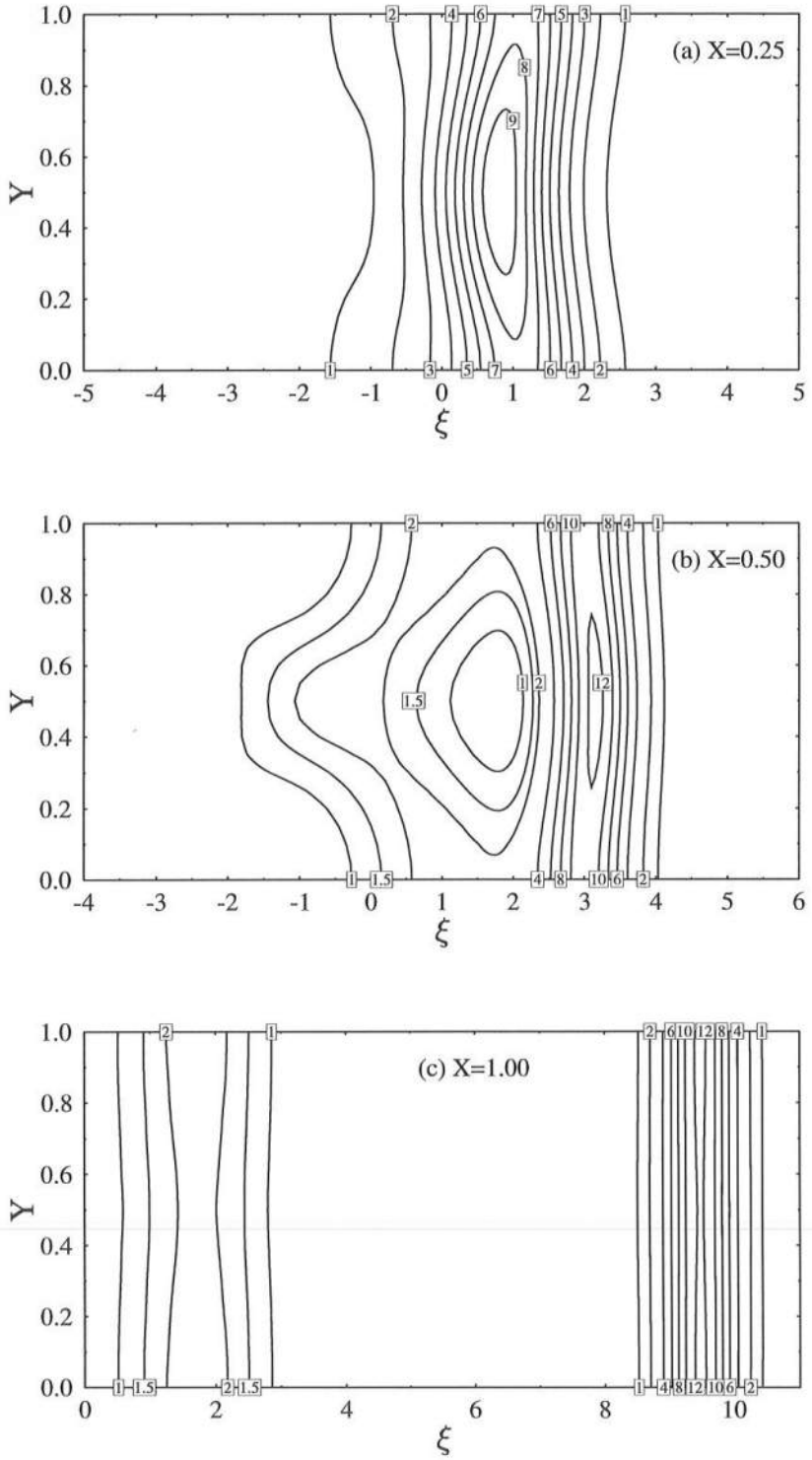

Figure 9: Contour plots of a normal incident solitary wave propagating over a 3-D shelf at different X.

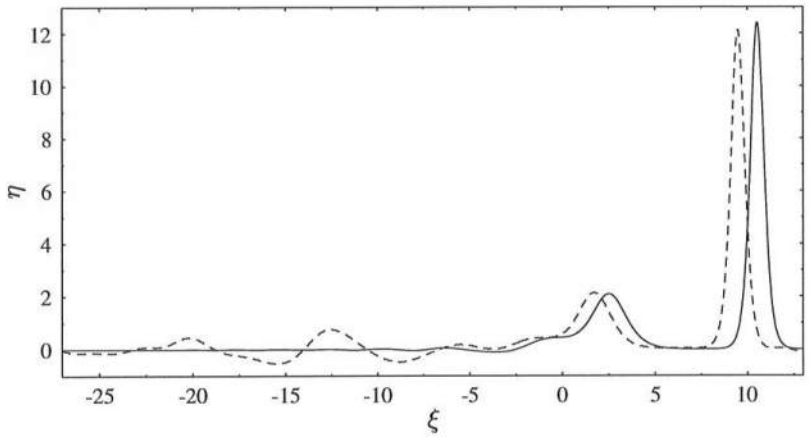

Figure 10: Centerline elevation of a normal incident solitary wave propagating over a 2-D shelf given by (3.3) and a 3-D shelf given by (3.4) at $X = 1.00$. ——, 2-D shelf; - - -, 3-D shelf.

this particular shelf). Again, with proper shifts, the shapes of the two solitary waves evolved from the wave propagating over the 3-D shelf coincide with the shapes of those two solitary waves evolved from the wave propagating over the corresponding 2-D shelf. Thus, the weak transversal variation of the shelf only alters the phase of each of the final 2-D solitary waves by almost the same amount and does not affect their number and shapes. This should also be true for any incident solitary wave propagating over an arbitrary 3-D shelf in a straight channel. Therefore, we can further generalize the claim given in the previous subsection as follows: an oblique incident (includes normal incident as a special case) solitary wave (with a smaller angle of incidence than the critical angle for the Mach reflection to occur according to Miles' theory (1977a, b)) propagating over a 3-D shelf ($H = h(X) + \epsilon B(X, Y)$) in a straight channel will eventually develop into a series of uniform straight-crested solitary waves, trailed by a train of small oscillatory waves propagating upstream. Moreover, with proper phase shifts, the shapes of these final 2-D solitary waves agree with the shapes of those final solitary waves emerged from a corresponding normal

incident solitary wave propagating over the corresponding 2-D shelf ($H = h(X)$).

In this section, the rotation effect has been ignored. We shall study the effect of topographic variation on the propagation of a Kelvin solitary wave in a rotating channel in the following section.

4 Kelvin solitary wave propagation in a rotating channel

Katsis & Akylas (1987*b*) and Grimshaw & Tang (1990) used the rmKP equation to numerically investigate the rotation effect on the development of an initially straight-crested Kelvin solitary wave of depression and elevation in a uniform channel, respectively. They confirmed that the rotation gives rise to a solitary-like wave whose wavefront is curved back, in qualitative agreement with the experiments of Renouard, D'Hiéres & Zhang (1987) and Maxworthy (1983). Katsis & Akylas' numerical results also showed that the wave amplitude decays slowly as the disturbance propagates downstream. This indicates that the solitary-like wave is not a wave of permanent form and the observed attenuation in experiments is only partly caused by the viscous damping. The constant-coefficient rmKP equations solved by Katsis & Akylas and Grimshaw & Tang do not include the effect of topography. In this section, we shall investigate the influence of the topographic variation on the propagation of a Kelvin solitary wave (of elevation and depression) in a rotating channel by solving the variable-coefficient uKP equation numerically.

4.1 Kelvin solitary wave of depression

Note that when $D_{-2} = \rho^-/(h^-)^2 - \rho^+/(h^+)^2 < 0$, the single solitary-wave solution to the KdV equation for a two-layered system is a wave of depression. The initial

condition for a Kelvin solitary wave of depression is given by

$$\eta(\xi,0,Y) = -\mathrm{sech}^2\left[\frac{C}{2}\sqrt{\left(\frac{-3D_{-2}}{\alpha D_1}\right)}\xi\right]\exp\left(-\beta Y/C\right), \quad (D_{-2}<0), \tag{4.1}$$

which satisfies the constraint (2.5) at $X = 0$.

We now study the transformation of a Kelvin solitary wave of depression given by (4.1) propagating over a 2-D shelf given by

$$h^-(X) = \begin{cases} 3.25, & X \le 0, \\ 1.625\left[1.2 + 0.8\cos(\pi X/2)\right], & 0 < X \le 2, \\ 0.65, & X > 2, \end{cases} \tag{4.2}$$

in a channel with rotation $\beta = 0.6$ and upper-layer depth $h^+ = 0.5$. The densities of the upper and lower layers are assumed to be very close for the rigid-lid assumption to be valid, i.e. $\rho^- \approx \rho^+ \approx 1.0$. For comparison, we also show the results for the same incident wave propagating over a flat bottom $h^- = 3.25$ in the same channel. In numerical computations, $\Delta\xi = 0.16$, $\Delta\bar{Y} = 0.025$, $\Delta X = \frac{2}{3}\times 10^{-3}$ and $\alpha = 0.781$ have been used.

Figures 11(a) and 11(b) show the interfacial displacement of the Kelvin solitary wave propagating over the flat bottom and the 2-D shelf at $X = 3.2$ respectively, where in both cases the leading wave reaches what appears to be a stable shape, characterized by a curved-back front moving as a whole and trailed by a train of small-amplitude waves. However, the front does not have a permanent shape because the wave amplitude attenuates slowly as the disturbance propagates downstream. Comparing figure 11(a) with 11(b), one can see that the presence of the shelf increases the value of the maximum amplitude, increases the decay rates across the channel, but decreases the curvature of the leading wave crest. For more quantitative comparison, we plot different decay rates across the channel at $X = 3.2$ and the maximum wave

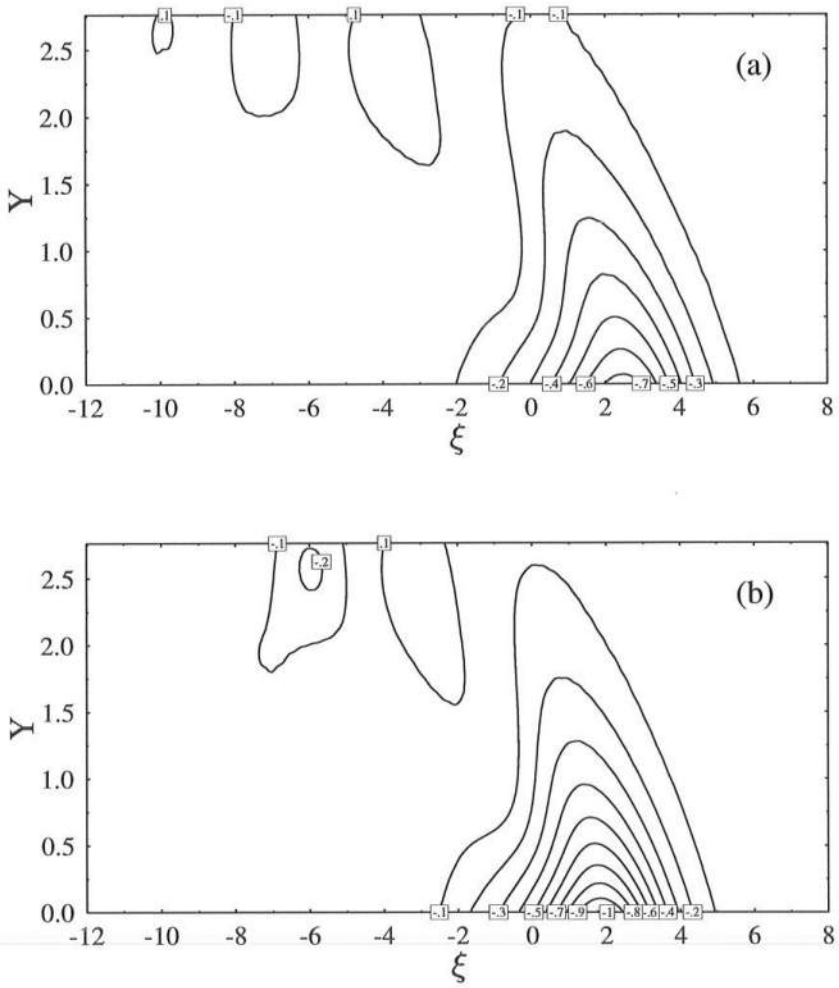

Figure 11: Interfacial displacement of a Kelvin solitary wave of depression propagating in a rotating channel with $\beta = 0.6$ at $X = 3.2$. (a) over a constant depth; (b) over a 2-D shelf.

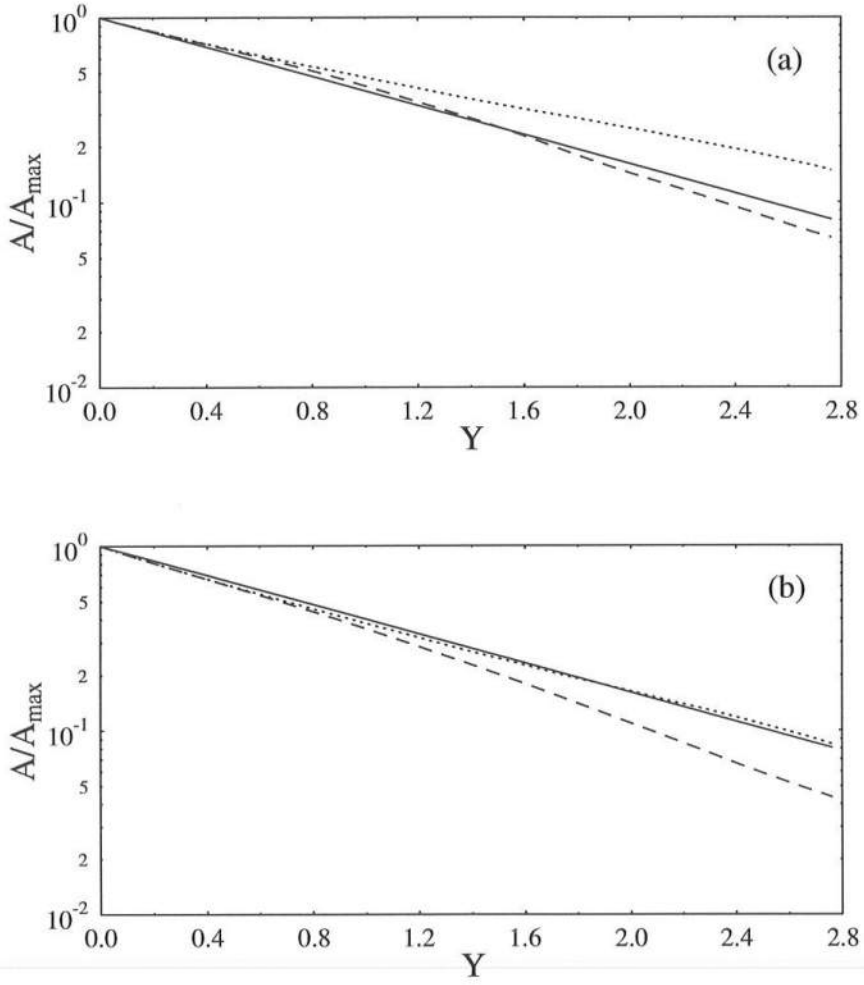

Figure 12: The decay rates of the wave amplitude across the channel in a rotating channel with $\beta = 0.6$. (a) over a constant depth; (b) over a 2-D shelf . - - -, in the plane perpendicular to the right-hand sidewall; $\cdots$, along the curved wave crest; ——, predicted by the linear theory.

amplitude along the right-hand sidewall for both cases.

Figure 12 shows the decay rates across the channel in the plane perpendicular to the right-hand sidewall passing through the point of maximum amplitude (dashed line) and along the wave crest (dotted line). In each case, the dotted line and dashed line are very close to straight lines; the dashed line is steeper than the dotted line. This indicates that the variations of the wave amplitude across the channel are nearly exponential and the decay rate along the plane perpendicular to the sidewall passing through the point of maximum amplitude is greater than that along the wave crest. Comparing figure 12(a) with 12(b), we observe that both decay rates increase by almost the same amount when the shelf is present. For comparison, the linear decay rate $\exp(-\beta Y/C)$ across the channel is also plotted in the figures (solid lines). The linear theory gives very good prediction of the decay rate along the wave crest when the shelf is present, whereas in the absence of the shelf, it gives a pretty good approximation for the decay rate in the plane perpendicular to the right-hand sidewall.

Figure 13 shows the maximum wave amplitude along the right-hand sidewall for the Kelvin solitary wave propagating over the constant depth and the 2-D shelf. In case of constant depth, the maximum amplitude monotonously decreases along the wall. On the other hand, when the shelf is present, the maximum amplitude along the wall first decreases until it reaches the minimum value at the middle of the shelf, and then increases until it reaches the maximum value near the top of the shelf. Once the wave enters to the constant depth region, its maximum amplitude gradually attenuates along the channel.

Next, we investigate the effect of a weak 3-D topography on the Kelvin solitary wave propagation in the same rotating channel. The bottom is given by

$$H^- = 3.25 + \epsilon B(X, Y), \tag{4.3a}$$

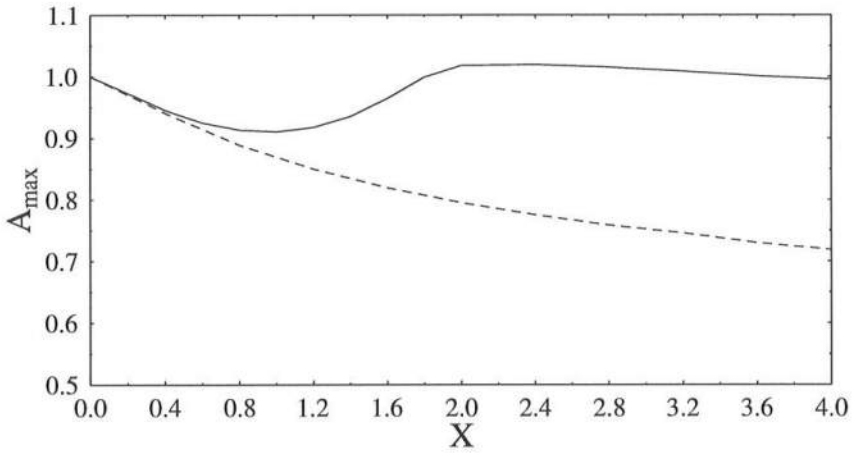

Figure 13: Maximum wave amplitude along the right-hand sidewall. ——, over a 2-D shelf; - - -, over a flat bottom.

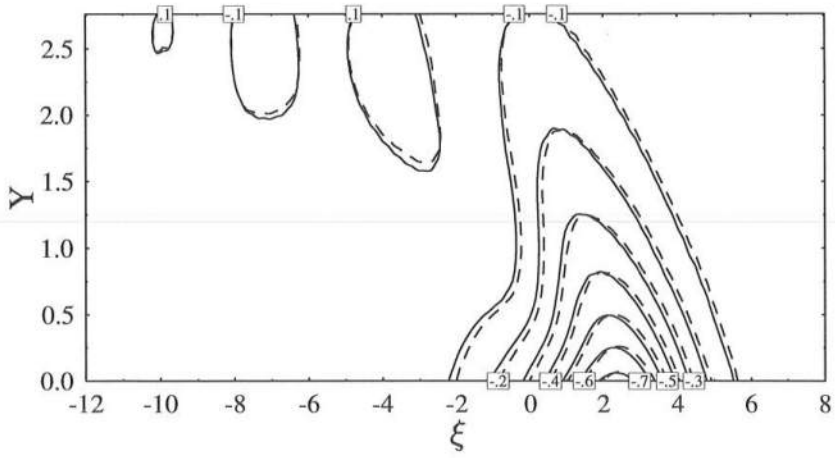

Figure 14: Contour plots of the interfacial displacement at $X = 3.2$ ($\beta = 0.6$). ——, over a weak 3-D topography given by (4.3); - - -, over a flat bottom.

where

$$B(X,Y) = 4\left[\cos(\pi X/2) - 1\right](Y - Y^2/2). \tag{4.3b}$$

Figure 14 shows the contour plots of the interfacial displacement at $X = 3.2$ for the Kelvin solitary wave propagating in the channel with the flat bottom ($H^- = 3.25$) and with the bottom given by (4.3). The variation of the weak topography only causes a slight time delay in the propagation of the leading wave. Thus, the effect of the weak 3-D bottom does not have much influence on the wave propagation.

According to the fission law for the variable-coefficient KdV equation in a two-layered system (Djordjevic & Redekopp 1978), with a small difference in densities, for a solitary wave of depression to undergo fission by decreasing the lower fluid depth, the greatest value of the ratio of the upper depth to the lower depth ahead of the shelf is about 0.07. For such small values of depth ratio allowing fission to occur, either the dispersion is not weak compared to the lower depth or the nonlinearity is too strong with respect to the upper depth. Thus, the KdV theory is not appropriate for describing fission of a solitary wave of depression propagating over a decreasing bottom. However, for a solitary wave of elevation, there is no strict limitation on the depth ratio for fission to occur.

It is understandable that the weak 3-D topography does not have much effect on the propagation of the Kelvin solitary wave of depression (see figure 14): the lower layer is much deeper than the upper layer and thus the wave barely detects the variation of the topography. However, comparing figure 11(a) with 11(b), we notice that the existence of the two-dimensional shelf given by (4.2), which reduces the lower depth by 80%, does not have a significant effect on the propagation of the Kelvin solitary wave of depression either, since the wave pattern still looks similar to the one without the presence of the shelf. Note that in the absent of rotation, the corresponding KdV solitary wave of depression does not undergo fission on passing over

the shelf. This implies that under the weak nonlinearity and dispersion assumption, the variation of an arbitrary topography does not have much effect on the propagation of a Kelvin solitary wave of depression in a rotating channel, because it cannot cause the corresponding KdV solitary wave to undergo fission. In the following subsection, we shall study how significant influence the topographic variation can have on the propagation of a Kelvin solitary wave of elevation, which can undergo fission easily in the absence of rotation without violating the weak nonlinearity and dispersion assumption.

4.2 Kelvin solitary wave of elevation

For a Kelvin solitary wave of elevation:

$$\eta = \operatorname{sech}^2\left[\frac{C}{2}\sqrt{\left(\frac{3D_{-2}}{\alpha D_1}\right)}\xi\right]\exp\left(-\beta Y/C\right), \quad (D_{-2} > 0), \tag{4.4}$$

propagating over a shelf given by

$$h^-(X) = \begin{cases} 0.5, & X \leq 0, \\ 0.25\left[1.6 + 0.4\cos(2\pi X)\right], & 0 < X \leq 0.5, \\ 0.3, & X > 0.5, \end{cases} \tag{4.5}$$

in a rotating channel with $h^+ = 1.0$, $\rho^+ \approx \rho^- \approx 1.0$, figure 15 shows the contour plot and 3-D plot of the interfacial displacement for $\beta = 0.25$ at $X = 5.4$, where the wave seems to reach a stable pattern: the leading wave is curved back, behind which the wave crests take turns to appear alternatingly along the left-hand sidewall and the right-hand sidewall (note that the heights of the first three crests behind the leading wave are not very small compared to that of the leading wave). However, the leading wave still decays gradually as it propagates downstream. In numerical computations,

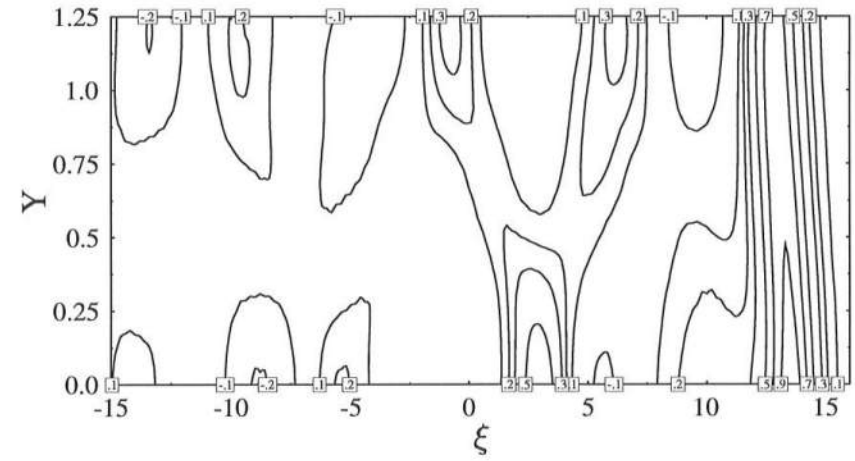

(*a*)

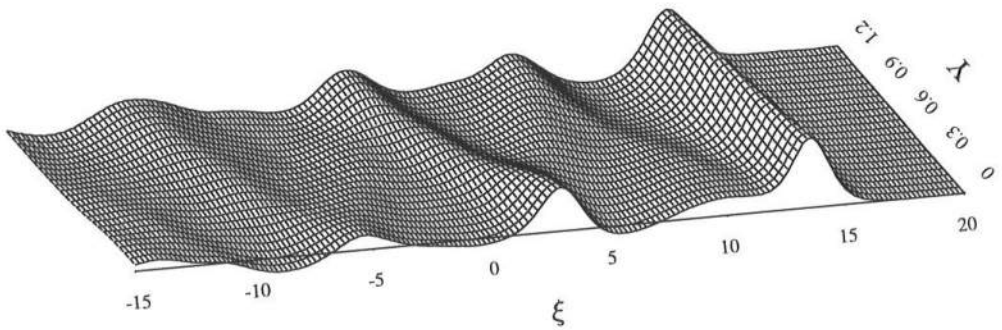

(*b*)

Figure 15: Interfacial displacement of an Kelvin solitary wave of elevation propagating over the shelf given by (4.5) in a rotating channel with $\beta = 0.25$ at $X = 5.4$. (*a*) Contour plot; (*b*) 3-D plot.

$\Delta\xi = 0.2$, $\Delta\bar{Y} = 0.0417$, $\Delta X = 0.2 \times 10^{-2}$ and $\alpha = 1.5$ have been used. For stronger rotation, similar wave pattern is also observed. Comparing the wave pattern shown in figure 15 with the counterpart for a flat bottom, which looks like the one shown in figure 11(a) under the transformation: $\eta \to -\eta$, we find that the existence of the shelf, which will cause the corresponding KdV solitary wave in the absence of rotation to disintegrate into two solitary waves, has a great influence on the propagation of the Kelvin solitary wave of elevation. Thus, the variation of topography can have a great impact on the propagation of a Kelvin solitary wave of elevation in a rotating channel if the corresponding KdV solitary wave can undergo fission, which, unlike in the case of Kelvin solitary wave of depression, is rather easy to occur.

5 Concluding remarks

In this paper, we have mainly investigated the effect of topographic variation on solitary wave propagation in a stationary channel and on Kelvin solitary wave propagation in a two-layered rotating channel by solving the variable-coefficient uKP equation numerically. The numerical scheme was developed based on the Petrov–Galerkin finite-element method for the KdV equation.

Through investigating solitary wave propagation in a stationary channel, we conclude that an oblique incident solitary wave (with an angle of incidence smaller than the corresponding critical angle for the Mach reflection to occur according to Miles' theory (1977a, b)) propagating over a three-dimensional shelf in a stationary straight channel will eventually develop into a series of uniform straight-crested solitary waves, trailed by a train of small oscillatory waves propagating upstream. Furthermore, with proper phase shifts, the shapes of these final two-dimensional solitary waves coincide with the shapes of those final solitary waves evolved from a corresponding normal incident solitary wave propagating over the corresponding two-dimensional

shelf. Therefore, if only the final solitary waves are relevant, we only need to solve the corresponding KdV equation instead of the uKP equation, which will dramatically reduce the computational effort. The two-dimensional adjustment process in the wave propagation, which occurs not only in a channel with a flat bottom but also in a channel with a 2-D topography, is attributed to the alternating development of stem waves along the left and the right sidewalls, which gradually reduces the amplitude and speed differences between the waves along both sidewalls and eventually leads to the formation of uniform straight-crested solitary waves spanning the entire channel width. The weak topographic variation in the transversal direction (finite portion in terms of the slow coordinate X) only alters the phase of each of the final 2-D solitary waves by almost the same amount and does not affect their number and shapes.

By studying the propagation of a Kelvin solitary wave in a two-layered rotating channel, we have found that in a rotating channel, the variation of topography has little effect on the propagation of a Kelvin solitary wave of depression: the wave patterns look similar with or without the presence of a shelf, whereas it may have a significant influence on the propagation of a Kelvin solitary wave of elevation. The reason is that in the absence of rotation, the corresponding KdV solitary wave of depression cannot experience fission under the weak nonlinearity and dispersion assumption, whereas the solitary wave of elevation can easily undergo fission without violating this assumption.

Finally we would like to make following comments:

- Through a linear stability analysis of the KP equation, Kadomtsev & Petviashvili (1970) and Oikawa, Satsuma & Yajima (1974) showed that the single solitary-wave solution to the KdV equation is neutrally stable subjected to small, transverse perturbations. Our numerical results have demonstrated that solitary wave solutions to the KdV equation are stable even with respect to any

moderate, 3-D disturbance, for which the linear stability analysis is no longer valid.

- The 2-D adjustment mechanism, which takes a longer time in a wider channel, is also responsible for the upstream generation of uniform straight-crested solitary waves in uniform channels by moving three-dimensional sources (Katsis & Akylas 1987*a*; Pedersen 1988; Hanazaki 1994) and suggests that no uniform straight-crested solitary wave will be generated if the width of the channel goes to infinity. We stress that the formation of uniform straight-crested solitary waves is the result of alternating development of stem waves along both sidewalls of the channel. In contrast to the implication of these authors, the adjustment process usually does not end after the first formation of a straight-crested wave because the wave is usually not uniform and the adjustment process continues until uniform straight-crested solitary waves form.

- The greatest limitation of using the uKP equation to study far-field wave behavior is that the initial condition must satisfy the constraint (2.5) at $X = 0$, which severely narrows the range of application of the uKP equation.

Acknowledgements

This research reported here was supported, in part, by Army Research Office (DAAL 03-92-G-0116) through a grant to Cornell University. YC completed this manuscript at CCS/SIO while supported by a Mellon Foundation grant.

References

Ablowitz, M.J. & Clarkson, P.A. 1991. *Solitons, Nonlinear Evolution Equations and Inverse Scattering.* Cambridge University Press.

Akylas, T.R. 1994. Three-dimensional long water-wave phenomena. *Ann. Rev. Fluid Mech.* **26**, 191–210.

Chen, Y. 1995. *Modelling of surface water wave and interfacial wave propagation.* Ph. D. thesis, Cornell University.

Chen, Y. & Liu, P. L.-F. 1995. The unified Kadomtsev–Petviashvili equation for interfacial waves. *J. Fluid Mech.* in press.

Djordjevic, V.D. & Redekopp, L.G. 1978. The fission and disintegration of internal solitary waves moving over two-dimensional topography. *J. Phys. Oceanogr* **8**, 1016–1024.

Grimshaw, R. & Melville, W.K. 1989. On the derivation of the modified Kadomtsev–Petviashvili equation. *Stud. Appl. Math.* **80**, 183–202.

Grimshaw, R. & Tang, S. 1990. The rotation-modified Kadomtsev–Petviashvili equation: An analytical and numerical study. *Stud. Appl. Math.* **83**, 223–248.

Hanazaki, H. 1994. On the three-dimensional internal waves exited by topography in the flow of a stratified fluid. *J. Fluid Mech.* **263**, 293–318.

Johnson, R.S. 1972. Some numerical solutions of a variable-coefficient Korteweg–de Vries equation. *J. Fluid Mech.* **54**, 81–91.

Johnson, R.S. 1973. On the development of a solitary wave moving over an uneven bottom. *Proc. Camb. Phil. Soc.* **73**, 183–203.

Kadomtsev, B.B. & Petviashvili, V.I. 1970. On the stability of solitary waves in weakly dispersing media. *Sov. Phys. Dokl.* **15**, 539–541.

Katsis, C. & Akylas, T.R. 1987a. On the excitation of long nonlinear water waves by a moving pressure distribution. Part 2. Three-dimensional effects. *J. Fluid Mech.* **177**, 49–65.

Katsis, C. & Akylas, T.R. 1987b. Solitary internal waves in a rotating channel: A numerical study. *Phys. Fluids* **30**(2), 297–301.

Maxworthy, T. 1983. Experiment on solitary internal kelvin waves. *J. Fluid Mech.* **129**, 365–383.

Methew, J. & Akylas, T.R. 1990. On three-dimensional long water waves in a channel with sloping sidewalls. *J. Fluid Mech.* **215**, 289–307.

Miles, J.W. 1977a. Obliquely interacting solitary waves. *J. Fluid Mech.* **79**, 157–169.

Miles, J.W. 1977b. Resonantly interacting solitary waves. *J. Fluid Mech.* **79**, 171–179.

Mitchell, A.R. & Schoombie, W. 1984. Finite element studies of solitons. In R. Lewis, P. Bettess, and E. Hinton (Eds.), *Numerical Methods in Coupled Systems*, pp. 465–488. John Wiley & Sons.

Oikawa, M., Satsuma, J. & Yajima, N. 1974. Shallow water waves propagating along undulation of bottom surface. *J. Phys. Soc. Japan* **37**, 511–517.

Ono, H. 1972. Wave propagation in an inhomogeneous anharmonic lattice. *J. Phys. Soc. Japan* **32**, 332–336.

Pedersen, G. 1988. Three-dimensional waves patterns generated by moving disturbances at transcritical speeds. *J. Fluid Mech.* **196**, 39–63.

Pierini, S. 1986. Solitons in a channel emerging from a three-dimensional initial wave. *Il Nuovo Cimento* **9C**(6), 1045–1061.

Renouard, D.P., D'Hiéres, G.C. & Zhang, X. 1987. An experimental study of strongly nonlinear waves in a rotating system. *J. Fluid Mech.* **177**, 381–394.

Sanz-Serna, J.M. & Christie, I. 1981. Petrov–Galerkin methods for nonlinear dispersive waves. *J. Comput. Phys.* **39**, 94–102.

Taha, T.R. & Ablowitz, M.J. 1984. Analytical and numerical aspects of certain nonlinear evolution equations. III. Numerical, Korteweg–de Vries equation. *J. Comput. Phys.* **55**, 231–253.

Tappert, F. & Zabusky, N.J. 1971. Gradient-induced fission of solitons. *Phys. Rev. Lett.* **27**, 1774–1776.

Wineberg, S.B., McGrath, J.F., Gabl, E.F., Scott, L.R. & Southwell, G.E. 1991. Implicit spectral methods for wave propagation problems. *J. Comput. Phys.* **97**, 311–336.